I.O.S.

# A RE–ANALYSIS OF SWOP DATA

BY

M. A. SROKOSZ, P. G. CHALLENOR

AND A. D. MARGETTS

REPORT NO. 195

1985

NATURAL ENVIRONMENT RESEARCH COUNCIL

INSTITUTE OF OCEANOGRAPHIC SCIENCES

I.O.S.

# A RE–ANALYSIS OF SWOP DATA

BY

M. A. SROKOSZ, P. G. CHALLENOR

AND A. D. MARGETTS

REPORT NO. 195

1985

NATURAL ENVIRONMENT RESEARCH COUNCIL

INSTITUTE OF OCEANOGRAPHIC SCIENCES

INSTITUTE OF OCEANOGRAPHIC SCIENCES

WORMLEY

# A re-analysis of SWOP data

by

M.A. Srokosz, P.G. Challenor

and A.D. Margetts*

I.O.S. Report No. 195

1985

* *Present address:*

*3 Ullswater Close*
*Liden*
*Swindon*
*WILTS. SN3 6LH*

## 1. INTRODUCTION

This report arises out of work carried out by two of the authors (M.A.S. and P.G.C.) in connection with satellite radar altimeter measurements of surface waves (see Guymer et al, 1984). It became apparent during the course of that study that there exist considerable gaps in our knowledge of the spatial statistics of ocean waves. As radar altimeters sense the spatial characteristics of the wavefield at the sea surface (Barrick, 1972), a better understanding of the statistics is required to obtain useful wave information from the radar return. In particular, in order to verify theoretical results for wave parameters that might be derived from the radar return (for example, the new period parameter described by Challenor, 1984; or the skewness parameters described by Srokosz, 1984b), it is necessary to obtain accurate measurements of the spatial statistics of the wavefield.

Conventional measurements of waves, such as those made using a waverider buoy or shipborne wave recorder, give a time series of the sea surface elevation at a single point in space. This approach is clearly inadequate for the purposes of deriving spatial information about the waves. It is of course possible to obtain spatial wave information by using an array of wave measuring devices, but this is difficult to do. Furthermore, such an array will have limited spatial resolution unless a large number of devices are used, which is prohibitively expensive. Another problem with conventional measuring techniques is the question of whether they correctly measure nonlinear wave effects, such as skewness (see Srokosz, 1984a, for a discussion of these problems in relation to surface following buoys). As sea surface skewness is one of the wave parameters that we want to measure it is necessary to find an alternative measuring technique.

At the present time there appear to be four methods of obtaining spatial wave information, these are:

a. radar measurements

b. laser profilometry (see McLain, Chen & Hart, 1984)

c. photography (see Stilwell & Pilon, 1974)

d. stereo-photography (see Holthuijsen, 1983).

All these might be considered as remote sensing methods.

After investigating the various methods it seemed that the most promising one, for obtaining spatial wave information, was stereo-photography of the sea surface. Previous studies using stereo-photography have concentrated on obtaining the two-dimensional wave number spectrum from the surface elevation data (see Chase et al., 1957; Holthuijsen, 1983) and have not really examined statistics in the spatial domain. In view of this, and of the fact that stereo-photography over the ocean is not a simple technique, it seemed necessary to gain some experience in analysing such data as are available, in order to check whether it is possible to derive the required statistics. The most readily available data for such an exercise are those taken during the Stereo Wave Observation Project (SWOP, see Chase et al., 1957).

This report describes the re-analysis of the SWOP data to obtain spatial wave statistics. We begin, in section 2, by giving a description of the data and follow this in section 3 with a brief resumé of the details of the comparison between data and theory. Finally, in section 5, the conclusions of this study are given together with suggestions for further work using stereo-photography to study the spatial statistics of waves.

## 2. DESCRIPTION OF THE SWOP DATA

The method used to obtain stereo-photographs of the sea surface during SWOP is fully described by Chase et al. (1957) and the description will not be repeated here. Suffice to say that despite (or because of) various problems in obtaining and analysing the data SWOP resulted in two stereo-pairs suitable for analysis. These were analysed to provide surface elevation data on a 60 x 90 grid with a grid spacing of 9.144m (30 feet); this grid spacing being chosen to give a desired spectral resolution (Chase et al., 1957). It was found that the data contained a tilt relative to the reference plane (possibly due to the orientation of the cameras when the photographs were taken), which had to be removed to level the data. The levelled data are given in Tables 9.1 and 9.2 of Chase et al. (1957) and are used in this report (following Chase et al. 1957, they will be described as datasets 2 and 3). The data are given approximately in feet (it is necessary to divide by 1.016 to obtain feet exactly) but we have converted them to metres for the purpose of this analysis.

It should be said that even the levelled data given in Chase et al. (1957) contains errors. This is due to such effects as film shrinkage affecting the accuracy of surface elevation measurements. The accuracy of the height measurements is given by Chase et al. (1957) as $\pm$ 15.24cm ($\pm$ 6"). However, as this is only a preliminary study aimed at developing analysis techniques for stereo-photographic wave data we will not concern ourselves with these errors and assume that the data are accurate. The errors are fully discussed by Chase et al. (1957).

Having transferred the data from the SWOP report (Chase et al., 1957) to the computer it was first contoured (figures 1 and 2) and compared with the contour maps given by Chase et al. (1957, figure 11.4 and 11.5). By using the

same contour interval (60cm = 1.97 feet) as that used by Chase et al.(1957) it was possible to compare the maps directly and this provided a check that the data had been transferred correctly. Thus the theoretical analysis, described in the next section, could be applied to the data.

## 3. THEORY

A theoretical description of the sea surface, as a Gaussian random surface, was originally given by Longuet-Higgins (1957). More recently there have been many different approaches applied to the study of random surfaces (or fields) and these are described by Adler (1981) and Vanmarcke (1983). However, for our purposes the original work of Longuet-Higgins (1957) and its extension to allow for weakly nonlinear wave effects (Longuet-Higgins, 1963) will be adequate.

Longuet-Higgins (1957) showed that the statistical properties of the sea surface depend on the statistical movements of the surface elevation $\zeta$ and its spatial and temporal derivatives (that is, $\zeta_x$, $\zeta_y$, $\zeta_{xy}$, ... and $\zeta_t$, $\zeta_{tt}$ ...). Here, as we are concerned with a fixed moment in time, we will only consider $\zeta$ and its spatial derivatives. If nonlinear wave effects are important then the Gaussian theory is inadequate to describe the statistics. However, Longuet-Higgins (1963; see also Srokosz 1984b) has extended the theory to allow for weakly nonlinear wave effects and the resulting non-Gaussian theory will also be used here.

As stated in the introduction the original interest in the spatial statistics of the sea surface arose from attempts to understand the wave measuring capabilities of pulse-limited radar altimeters. It was found (see Guymer et al., 1984; Challenor & Srokosz 1984; Srokosz, 1984b) that the form of the radar return depended on the statistical moments of the surface elevation $\zeta$ and its first derivatives $\zeta_x$, $\zeta_y$. These moments are given by

$$\mu_{mnp} = \left\langle \zeta^m \zeta_x^n \zeta_y^p \right\rangle \qquad (3.1)$$

where $\langle\ \rangle$ denotes the ensemble average. It is convenient to work with normalised moments, elevation and slopes, given by

$$\left.\begin{aligned} \lambda_{mnp} &= \mu_{mnp} \,/\, \mu_{200}^{m/2}\ \mu_{020}^{n/2}\ \mu_{002}^{p/2} \\ \eta &= \zeta/\mu_{200}^{1/2}\ ,\ \eta_x = \zeta_x/\mu_{020}^{1/2}\ ,\ \eta_y = \zeta_y/\mu_{002}^{1/2} \end{aligned}\right\} \qquad (3.2)$$

The parameters of particular relevance to radar altimeter wave studies (see papers cited above) are:

$\mu_{200}$ - the variance of the sea surface elevation $\zeta$

(significant wave height $H_s = 4\,\mu_{200}$)

$\mu_{020}, \mu_{002}$ - the variances of the surface slopes $\zeta_x$, $\zeta_y$

$\mu_{011}$ - the covariance of the surface slopes $\zeta_x$, $\zeta_y$

$\lambda_{300}$ - the skewness of the sea surface elvation $\zeta$

$\lambda_{120}, \lambda_{102}, \lambda_{111}$ - various cross-skewness coefficients

(of unknown physical significance).

In fact, some of these do not appear individually in the theory but in the following combinations.

$$\Delta_2 = (\mu_{020}\mu_{002} - \mu_{011}^2) \qquad (3.3)$$

$$\delta = (\lambda_{102} + \lambda_{120} - \lambda_{011}\,\lambda_{111})/(1-\lambda_{011}^2) \qquad (3.4)$$

and are important physical parameters (see Challenor & Srokosz, 1984, and Srokosz, 1984b). $\Delta_2$ is a measure of the slope variance and may be related to the fourth moment of the wave frequency spectrum (Challenor, 1984). $\delta$ is important for estimating the sea state bias (that is, the error in mean sea level determination due to nonlinear wave effects) of the radar altimeter measurements (Srokosz, 1984b).

From the results of Longuet-Higgins (1957, 1963) it can be shown that the pdf of the sea surface elevation $\zeta$ is given by

$$p(\zeta) = \frac{1}{\sqrt{2\pi\mu_{200}}} \exp\left\{-\tfrac{1}{2}\eta^2\right\}$$

(3.5) in the Gaussian case, and

$$p(\zeta) = \frac{1}{\sqrt{2\pi\mu_{200}}} \exp\left\{-\tfrac{1}{2}\eta^2\right\}\left[1 + \frac{1}{6}\lambda_{300}\left(\eta^3 - 3\eta\right)\right] \tag{3.6}$$

in the non-Gaussian case. To the same order of approximation for the non-Gaussian case the pdf's of the surface slopes $\zeta_x$ and $\zeta_y$ are the same as those for the Gaussian case (Srokosz, 1984b) and are given by

$$p(\zeta_x) = \frac{1}{\sqrt{2\pi\mu_{020}}} \exp\left\{-\tfrac{1}{2}\eta_x^2\right\} \tag{3.7}$$

and

$$p(\zeta_y) = \frac{1}{\sqrt{2\pi\mu_{002}}} \exp\left\{-\tfrac{1}{2}\eta_y^2\right\} \tag{3.8}$$

We will not consider the joint distribution of $\zeta$, $\zeta_x$ and $\zeta_y$ as the data are not adequate either in quality or quantity, to obtain a reasonable estimate of this pdf (for relevant theory see Longuet-Higgins, 1957 and Srokosz, 1984b).

Another parameter for which it is possible to make a comparison between the theory and data is the mean length of contours per unit area $\bar{s}$ at a given level $\zeta$. Longuet-Higgins (1957) showed that for a Gaussian surface

$$\bar{s} = \frac{1}{\pi}\left(\frac{\mu_{020} + \mu_{002}}{\mu_{200}}\right)^{\frac{1}{2}} \exp\left\{-\tfrac{1}{2}\eta^2\right\} \times \left(1+\gamma^2\right)^{-\frac{1}{2}} E\left(\sqrt{1-\gamma^2}\right) \tag{3.9}$$

where the long-crestedness parameter $\gamma^{-1}$ is given by

$$\gamma^2 = \frac{\left(\mu_{020} + \mu_{002}\right) - \sqrt{\left(\mu_{020} - \mu_{002}\right)^2 + 4\mu_{011}^2}}{\left(\mu_{020} + \mu_{002}\right) + \sqrt{\left(\mu_{020} - \mu_{002}\right)^2 + 4\mu_{011}^2}} \tag{3.10}$$

and $E(.)$ is the complete elliptic integral of the second kind.

A similar result for the non-Gaussian case can be derived from the work of Srokosz (1984b) and can be written, in principal axes form, as

$$\bar{s} = \frac{1}{\pi}\left(\frac{\mu_{020}+\mu_{002}}{\mu_{200}}\right)^{\frac{1}{2}}(1+\gamma^2)^{-\frac{1}{2}}\left[\left\{1+\frac{1}{6}\lambda_{300}\eta^3 - \frac{1}{2}\eta\left(\lambda_{300}+\lambda_{120}+\lambda_{102}\right)\right\} E\left(\sqrt{1-\gamma^2}\right)\right.$$

$$+\frac{1}{2}\eta\gamma^2\left\{\lambda_{102}\left[K\left(\sqrt{1-\gamma^2}\right)+\left(\frac{2\gamma^2-1}{\gamma^2}\right)E\left(\sqrt{1-\gamma^2}\right)\right]\right.$$

$$\left.\left.+\lambda_{120}(1-\gamma^2)^{-1}\left[\left(\frac{2-\gamma^2}{\gamma^2}\right)E\left(\sqrt{1-\gamma^2}\right)-K\left(\sqrt{1-\gamma^2}\right)\right]\right\}\right]$$

$$\times \exp\left\{-\frac{1}{2}\eta^2\right\} \qquad (3.11)$$

where K(.) is the complete elliptic interal of the first kind. (For the derivation of this result see the appendix). We note that in the above the parameters $\mu_{200}$, $(\mu_{020}+\mu_{002})$, $\Delta_2$, $\lambda_{300}$ and $\gamma$ are invariant under transformation of axes.

In the following section we will compare results obtained from the SWOP data with the theoretical ones outlined above. There are, of course, many other theoretical results that could be tested against the data and the above have been chosen primarily for illustrative purposes.

## 4. ANALYSIS AND RESULTS

In order to calculate the various parameters mentioned in the previous section it is necessary to know the x and y derivatives of the surface elevation $\zeta$. These can be calculated from the data by a variety of methods. Three methods were tried: linear interpolation (first differences), Fourier interpolation (FFT) and bi-cubic spline interpolation. Figures 3 and 4 show plots of the surface elevation $\zeta$ along sections through the surface of dataset 2 in the x and y directions, respectively. Figures 5 and 6 show the corresponding x and y derivatives calculated along those sections. Although graphically the difference between the values calculated by the three methods is small, they lead to different results for some of the associated parameters (see Tables 1 and 2). In particular, those parameters that involve moments of $\zeta_x$ and $\zeta_y$ (that is, $\mu_{020}$, $\mu_{002}$, $\mu_{011}$ and $\delta$) show considerable variation. This may be explained by noting that the spatial resolution (with a grid spacing of 9.144m) is very poor, so that accurate estimates of the derivatives are difficult to obtain from the data. To proceed with the comparisons between data and theory it was decided to use the bi-cubic spline interpolated results as these appeared to give the smoothest fit to the data.

First of all the pdf's of the surface elevation $\zeta$ were estimated from the data and the results compared with the Gaussian and non-Gaussian pdf's given in equations (3.3) and (3.6). Here,and in subsequent comparisons, the parameters used in the theory were estimated from the data. Figures 7 and 8 show the comparison for datasets 2 and 3, respectively. It can be seen that the Gaussian theory provides a good fit to the data, while allowing for nonlinear wave effects (through the skewness $\lambda_{300}$) makes little difference. In fact, for dataset 3 the Gaussian and non-Gaussian results cannot be distinguished.

In figures 9 to 12 the result for the pdf's of the slopes $\zeta_x$ and $\zeta_y$ for both datasets are compared with the theoretical results (3.7) and (3.8). It can be seen that the fit is less good than that for the surface elevation $\zeta$. The data show a higher percentage of flatter slopes and a lower percentage of steeper slopes than might be expected theoretically. However, as pointed out above, the poor spatial resolution of the data will make the calculation of the derivatives less accurate. In particular, it will not be possible to resolve shorter steeper waves and so the difference between the data and the theory is perhaps due to this. We note that the variance of the y-derivatives $\mu_{002}$ is larger than that of the x-derivatives $\mu_{020}$ for both datasets indicating a definite directionality in the wavefield (for an isotropic wavefield $\mu_{020} = \mu_{002}$ and $\gamma = 1$). This directionality can be perceived in the contour plots of the data, though it is by no means obvious.

Finally, we will make a comparison between the contour lengths per unit area, at a given level $\zeta$, calculated from the data and those predicted theoretically from (3.9) and (3.11). To calculate the lengths of the contours we made use of a computer graphics contouring package , which was modified to measure the length of the contours plotted at a given level. The contour lengths were calculated at 0.2 metre intervals from $\zeta = -1$m to $\zeta = 1$m. The length of the contour at a given level was divided by the surface area of the contour map ($90 \times 60 \times (9.144)^2$ m$^2$ ) to obtain an estimate of $\bar{s}$. The results are given in Tables 3 and 4, together with the theoretical estimates of $\bar{s}$ from equations (3.9) and (3.11). For the non-Gaussian equation case, (3.11), principal axes results had to be calculated by rotation of axes to obtain maximum and minimum slope variances along the direction of the axes. This is a simple procedure computationally, so no details will be given.

It can be seen from the tables that while the qualitative agreement between the data and Gaussian theory is reasonable the quantitative agreement is less good. This is again possibly due to the poor resolution of the surface slopes in the data. From the tables it is also clear that the non-linear theory gives answers that differ slightly from the Gaussian case but the results do not allow any conclusions to be made about which theory is a better fit to the data.

## 5. CONCLUSIONS

It has been shown how stereophotographic data can be analysed to produce information about the spatial statistics of waves on the sea surface. It is clear from the analysis that the spatial resolution (9.144m) of the SWOP data is too poor to obtain conclusive answers to questions such as the importance of nonlinearity for the spatial statistics of waves. However, the analysis indicates that with better spatially resolved stereophotographic data it should be possible to calculate those parameters that are of interest; in particular those of importance in analysing the radar altimeter return signal from the sea surface.

It seems worthwhile therefore to pursue the use of stereophotography in the study of spatial wave statistics. In order to obtain better resolution than that obtained (temporally) from a waverider buoy it is necessary to have a spatial resolution of less than 1.5 metres (a waverider buoy has a temporal resolution of 1 sec., and this can be transformed to a spatial resolution via the dispersion relationship). If we assume a r.m.s. wave slope of 0.05 (not unreasonable in view of the data in Tables 1 and 2 for $\mu_{020}$ and $\mu_{002}$), this implies a necessary vertical resolution of 7.5cm in the stereophotographic data. In view of the advances made in stereophotography since the SWOP project of the 1950's, these are not unreasonable requirements. One further point that needs to be taken into account in any future stereophotographic study of ocean waves is the requirement to choose the correct size of area to photograph. This will clearly be determined by the wavenumber range that is of interest. A rough guide to the area that needs to be photographed is that it contains several (say 10) waves of the wavelength of interest. One technique that might be used to ensure good data at all scales (wavelengths) is that of taking

photographs of different size areas in order to resolve the different scales. Clearly careful planning of any stereophotographic experiment is required to ensure that the necessary data will be obtained.

ACKNOWLEDGEMENTS

We are grateful to Dr. Holthuijsen for pointing out to us the availability of the SWOP data and to Dr. Storey for advice and help in modifying the GRAFIX contouring routines used to calculate contour lengths.

## APPENDIX

The calculation of the mean contour length per unit area for a nonlinear random sea.

From Longuet-Higgins (1957) it can be seen that the mean contour length per unit area at a given level $\zeta$ is given by

$$\bar{s} = \int_0^{\infty} \int_0^{2\pi} \alpha \, p(\zeta, \alpha, \theta) \, d\theta \, d\alpha \tag{A.1}$$

where the surface slopes $\zeta_x, \zeta_y$ are given by

$$\zeta_x = \alpha \cos\theta \, , \; \zeta_y = \alpha \sin\theta$$

and $$p(\zeta, \alpha, \theta) \; d\alpha \; d\theta = p(\zeta, \zeta_x, \zeta_y) \; d\zeta_x \, d\zeta_y$$

where $p(\zeta, \zeta_x, \zeta_y)$ is the joint distribution of the surface elevation $\zeta$ and slopes $\zeta_x, \zeta_y$.

For a weakly nonlinear random sea Srokosz (1984b) has extended the work of Longuet-Higgins (1963) to show that

$$\begin{aligned} p(\zeta, \zeta_x, \zeta_y) = {} & (2\pi)^{-3/2} \mu_{200}^{-1/2} \left(\mu_{020}\mu_{002} - \mu_{011}^2\right)^{-1/2} \exp\left\{-\tfrac{1}{2}\eta^2\right\} \\ & \cdot \exp\left\{-\tfrac{1}{2}\left[\eta_x^2 - 2\eta_x\eta_y + \eta_y^2\right] / (1-\lambda_{011}^2)\right\} \\ & \cdot \left[1 + \tfrac{1}{6}\left(\lambda_{300} H_{300} + 3\left(\lambda_{120} H_{120} + \lambda_{102} H_{102} + 2\lambda_{111} H_{111}\right)\right)\right] \end{aligned} \tag{A.4}$$

where

$$\left.\begin{aligned} H_{300} &= \eta^3 - 3\eta \\ H_{120} &= \frac{\eta}{(1-\lambda_{011}^2)}\left[\frac{(\eta_x - \lambda_{011}\eta_y)^2}{(1-\lambda_{011}^2)} - 1\right] \\ H_{102} &= \frac{\eta}{(1-\lambda_{011}^2)}\left[\frac{(\eta_y - \lambda_{011}\eta_x)^2}{(1-\lambda_{011}^2)} - 1\right] \\ H_{111} &= \frac{\eta}{(1-\lambda_{011}^2)}\left[(\eta_x - \lambda_{011}\eta_y)(\eta_y - \lambda_{011}\eta_x)/(1-\lambda_{011}^2) + \lambda_{011}\right] \end{aligned}\right\} \tag{A.5}$$

Now in order to calculate $\bar{s}$ we need to make use of (A.1) to (A.5) and evaluate the resulting integral. To simplify this process we will follow Longuet-Higgins (1957) and work in principal axes coordinates, for which $\mu_{011} = \lambda_{011} = 0$. The resulting integral for $\bar{s}$ is given by

$$\bar{s} = (2\pi)^{-3/2} (\mu_{200}\mu_{020}\mu_{002})^{-1/2} \int_0^\infty \int_0^{2\pi} \alpha^2 \exp\{-\tfrac{1}{2}\eta^2\}$$
$$\cdot \exp\{-\tfrac{1}{2}\alpha^2 (\mu_{002}\cos^2\theta + \mu_{020}\sin^2\theta)/(\mu_{020}\mu_{002})\}$$
$$\cdot \Big[1 + \tfrac{1}{6}\lambda_{300}(\eta^3 - 3\eta) + \tfrac{1}{2}\lambda_{120}\eta\left(\frac{\alpha^2\cos^2\theta}{\mu_{020}} - 1\right)$$
$$+ \tfrac{1}{2}\lambda_{102}\eta\left(\frac{\alpha^2\sin^2\theta}{\mu_{002}} - 1\right) + \lambda_{111}\frac{\alpha^2\cos\theta\sin\theta}{\sqrt{\mu_{020}\mu_{002}}}\Big] d\theta\, d\alpha$$

Note that the final term (the one containing $\lambda_{111}$) is anti-symmetric in $\theta$ and therefore integrates to zero. The remaining terms can be integrated w.r.t. $\alpha$ to obtain

$$\bar{s} = \frac{\mu_{020}\mu_{002}}{4\pi\mu_{200}^{1/2}} \exp\{-\tfrac{1}{2}\eta^2\} \Big[1 + \tfrac{1}{6}\lambda_{300}\eta^3$$
$$- \tfrac{1}{2}\eta(\lambda_{300} + \lambda_{120} + \lambda_{102})\Big] \int_0^{2\pi} (\mu_{020}\sin^2\phi + \mu_{002}\cos^2\phi)^{-3/2} d\phi$$
$$+ \frac{3\mu_{020}\mu_{002}}{8\pi\mu_{200}^{1/2}} \eta \exp\{-\tfrac{1}{2}\eta^2\}$$
$$\cdot \int_0^{2\pi} \Big[\lambda_{102}\mu_{020}\sin^2\theta + \lambda_{120}\mu_{002}\cos^2\theta\Big] /$$
$$\Big[\mu_{002}\cos^2\theta + \mu_{020}\sin^2\theta\Big]^{5/2} d\theta$$

To evaluate the remaining integrals we use the results given by Gradshteyn & Ryzhik (1965, pp. 164,165) from which $\bar{s}$ can be written in terms of complete elliptic integrals of the first and second kind (K(.) and E(.)). The result obtained is given in equation (3.11).

## REFERENCES

Adler, R J 1981. The Geometry of Random Fields. John Wiley & Sons.

Barrick, D E 1972. Remote sensing of sea-state by radar, in Remote Sensing of the Troposphere, ed. V E Derr, ch. 12, U.S. Government Printing Office.

Chase, J Cote, L J Marks, W Mehr, E Pierson, W J Rönne, F C Stephenson, G Vetter, R C and Walden, R A 1957. The directional spectrum of a wind generated sea as determined from data obtained by the Stereo Wave Observation Project. College of Engineering, New York University.

Challenor, P G and Srokosz, M A 1984. Extraction of wave period from altimeter data, in 'ERS-1 Radar Altimeter Data Products' ed. Guyenne, T D and Hunt, J J ESA SP-221, pp 121-124.

Gradshteyn, I S and Ryzhik, I M 1965. Table of Integrals, Series and and Products. Academic Press.

Guymer, T H Challenor, P G Srokosz, M A Rapely, C G Queffeulou, P Carter, D J T Grifiths, H D McIntyre, N Scott, R F and Tabor, A R 1984. A study of ERS-1 radar altimeter data processing requirements. ESTEC Contract No. 5681/83/NL/BI.

Holthuijsen, L H 1983. Stereophotography of ocean waves. Appl. Ocean Res., vol. 5, pp. 204-209.

Longuet-Higgins, M S 1957. The statistical analysis of a random, moving surface. Phil. Trans. Roy. Soc. Lond., vol. A249, pp. 321-387.

Longuet-Higgins, M S 1963. The effect of nonlinearities on statistical distributions in the theory of sea waves. J. Fluid Mech., vol. 17, pp. 459-480.

McLain, C R Chen, D T and Hart, W D 1982. On the use of laser profilometry for ocean wave studies. J. Geophys. Res., vol. 87, pp. 9509-9515.

Srokosz, M A 1984a. On the skewness of the sea surface. (submitted for publication).

Srokosz, M A 1984b. On the joint distribution of surface elevation and slopes for a nonlinear random sea; with an application to radar altimetry. (submitted for publication).

Stilwell, D and Pilon, R O 1974. Directional spectra of surface waves from photographs. J. Geophys. Res., vol. 79, pp. 1277-1284.

Vanmarcke, E 1983. Random Fields. The M.I.T. Press.

TABLE 1

| | Bi-cubic spline | Linear | Fourier |
|---|---|---|---|
| $\mu_{200}$ | 0.425269 | 0.425269 | 0.425269 |
| $\mu_{020}$ | 0.002754 | 0.001272 | 0.004012 |
| $\mu_{002}$ | 0.004973 | 0.002139 | 0.006873 |
| $\mu_{011}$ | -0.000450 | -0.000373 | -0.000432 |
| $\lambda_{300}$ | 0.063447 | 0.061190 | 0.061190 |
| $\delta$ | 0.025427 | 0.051700 | -0.006520 |
| $\gamma$ | 0.725836 | 0.705530 | 0.754431 |

Results for dataset 2 using different methods for calculating spatial derivatives.

TABLE 2

| | Bi-cubic spline | Linear | Fourier |
|---|---|---|---|
| $\mu_{200}$ | 0.399246 | 0.399248 | 0.399248 |
| $\mu_{020}$ | 0.002646 | 0.001199 | 0.004040 |
| $\mu_{002}$ | 0.004609 | 0.001937 | 0.006344 |
| $\mu_{011}$ | -0.000316 | -0.000236 | -0.000303 |
| $\lambda_{300}$ | 0.002190 | -0.004941 | -0.004941 |
| $\delta$ | 0.072533 | 0.067909 | 0.036866 |
| $\gamma$ | 0.746545 | 0.750532 | 0.791691 |

Results for dataset 3 using different methods for calculating spatial derivatives.

TABLE 3

| $\zeta$ | $\bar{s}$ (data) | $\bar{s}$ (theory) | $\bar{s}$ (nonlinear theory) |
|---|---|---|---|
| 1.0 | 0.01108 | 0.01338 | 0.01324 |
| 0.8 | 0.01756 | 0.02043 | 0.01909 |
| 0.6 | 0.02753 | 0.02840 | 0.02682 |
| 0.4 | 0.03658 | 0.03592 | 0.03449 |
| 0.2 | 0.04369 | 0.04137 | 0.04107 |
| 0.0 | 0.04622 | 0.04336 | 0.04336 |
| -0.2 | 0.04328 | 0.04137 | 0.04168 |
| -0.4 | 0.03650 | 0.03592 | 0.03739 |
| -0.6 | 0.02748 | 0.02840 | 0.02999 |
| -0.8 | 0.01844 | 0.02043 | 0.02178 |
| -1.0 | 0.01067 | 0.01338 | 0.01325 |

Results for dataset 2, for the average contour length for unit area $\bar{s}$.

(Note:- $\zeta$ in metres, $\bar{s}$ in metres$^{-1}$ )

TABLE 4

| $\zeta$ | $\bar{s}$ (data) | $\bar{s}$ (theory) | $\bar{s}$ (nonlinear theory) |
|---|---|---|---|
| 1.0 | 0.01042 | 0.01240 | 0.01247 |
| 0.8 | 0.01720 | 0.01947 | 0.01954 |
| 0.6 | 0.02704 | 0.02764 | 0.02771 |
| 0.4 | 0.03652 | 0.03551 | 0.03557 |
| 0.2 | 0.04270 | 0.04127 | 0.04131 |
| 0.0 | 0.04471 | 0.04339 | 0.04339 |
| -0.2 | 0.04179 | 0.04127 | 0.04125 |
| -0.4 | 0.03498 | 0.03551 | 0.03546 |
| -0.6 | 0.02606 | 0.02764 | 0.02758 |
| -0.8 | 0.01730 | 0.01947 | 0.01940 |
| -1.0 | 0.01065 | 0.01240 | 0.01234 |

Results for dataset 3, for the average contour length per unit area $\bar{s}$.

(Note:- $\zeta$ in metres, $\bar{s}$ in metres$^{-1}$)

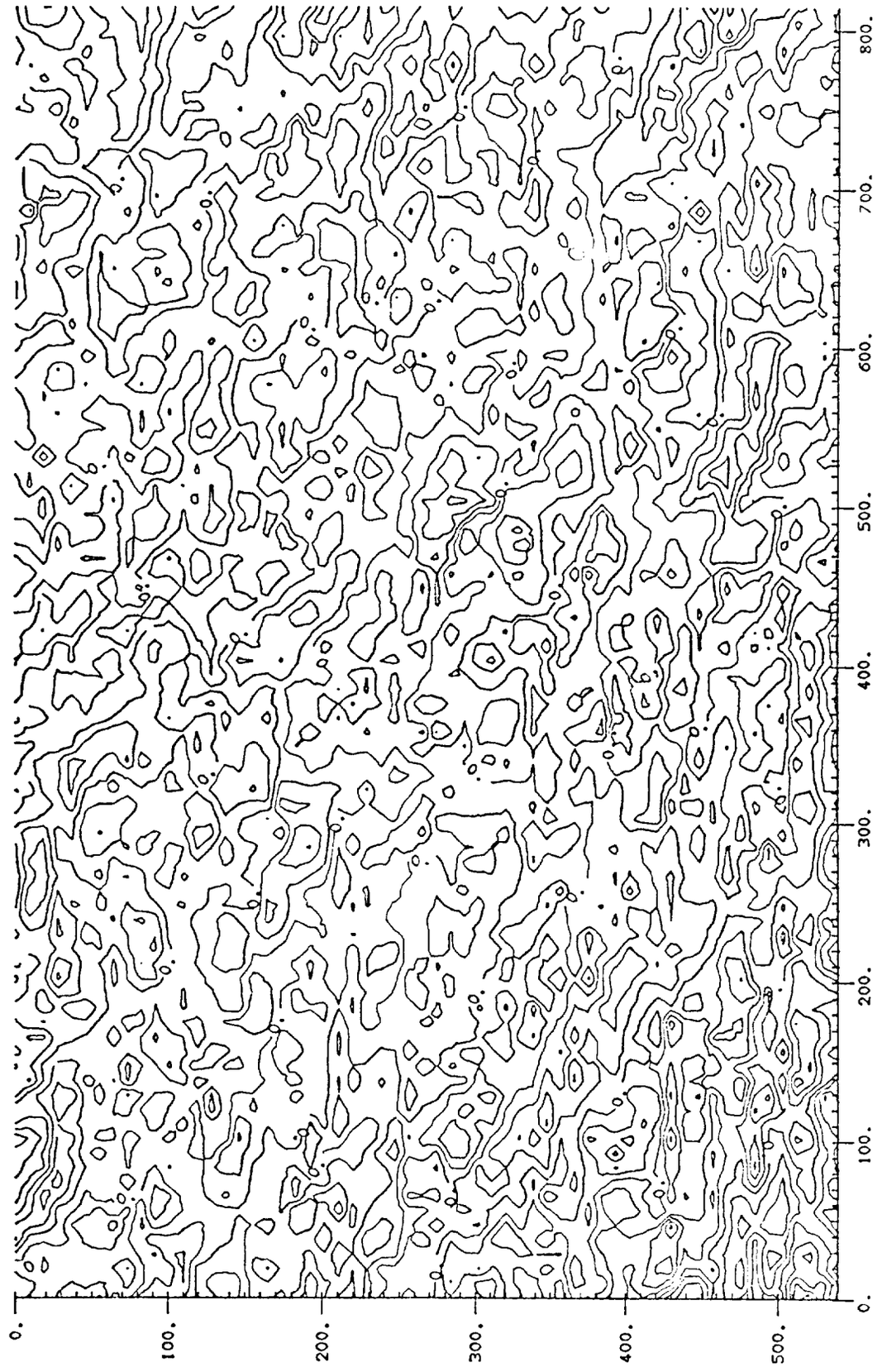


1. Contour plot of dataset 2. Contour interval 60cm (= 1.97 ft)

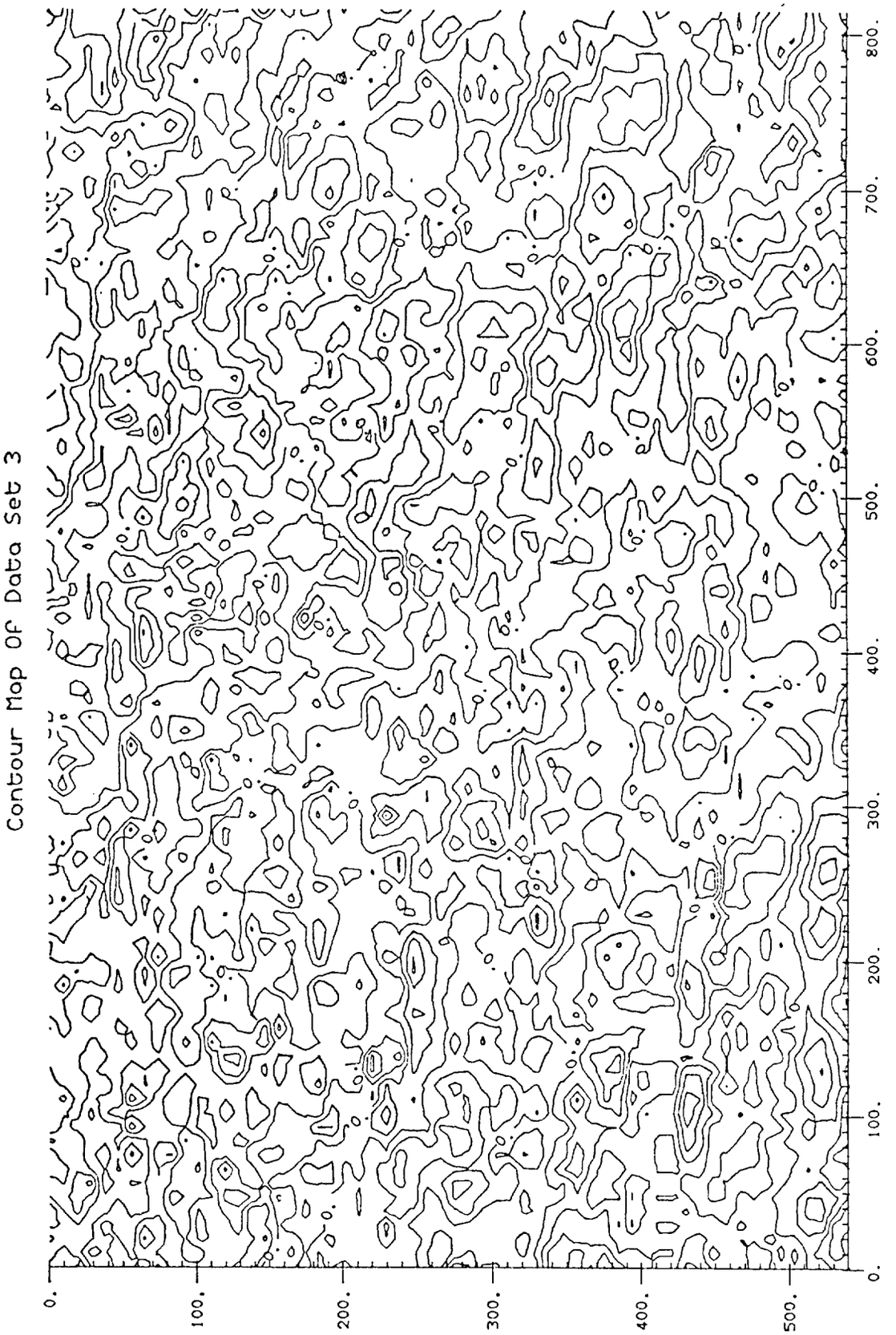


2. Contour plot of dataset 3. Contour interval 60cm (= 1.97 ft)

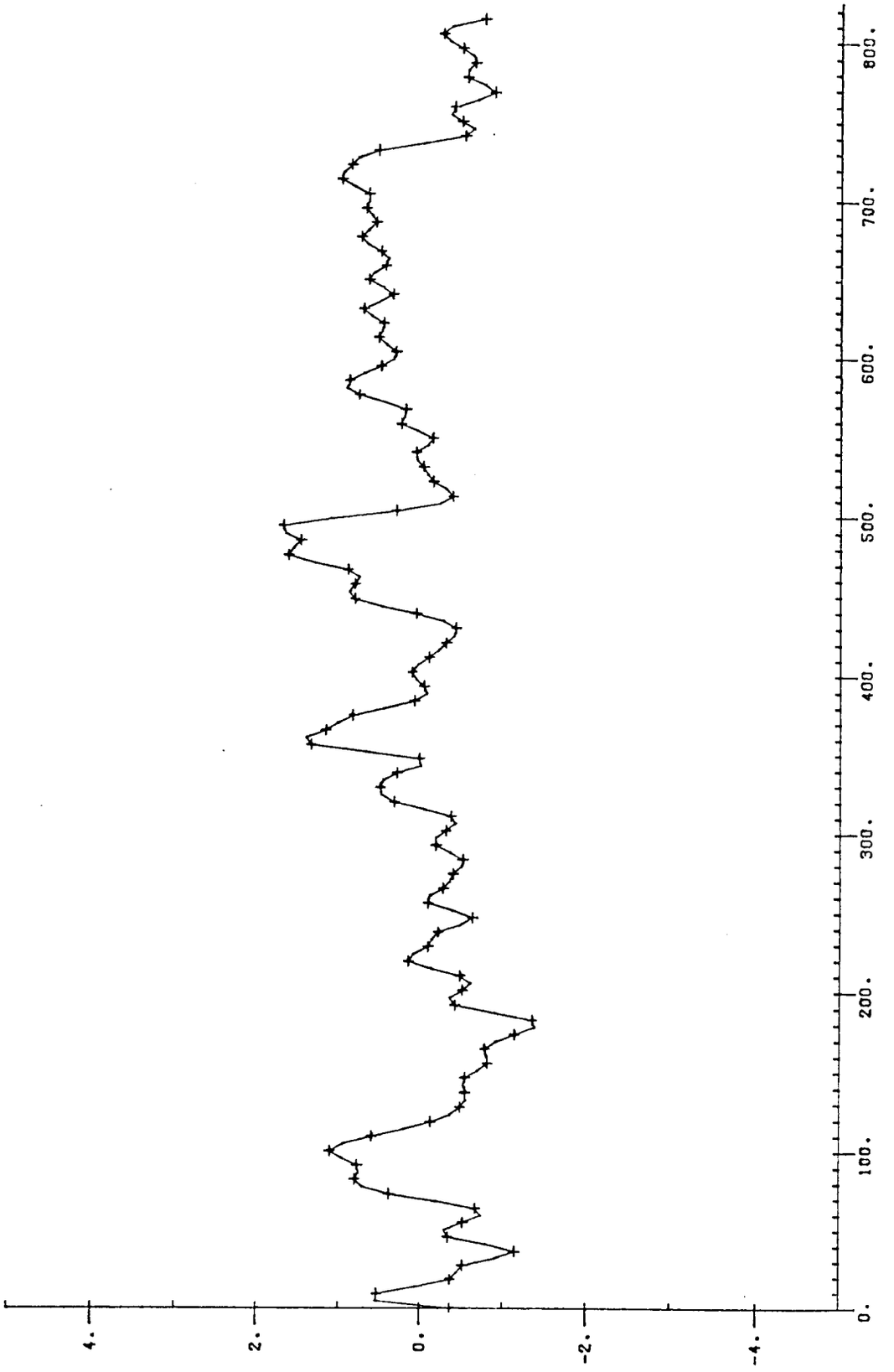


3. Bi-cubic spline interpolation of data (+) along line parallel to x-axis (y-grid coordinate 43), for dataset 2

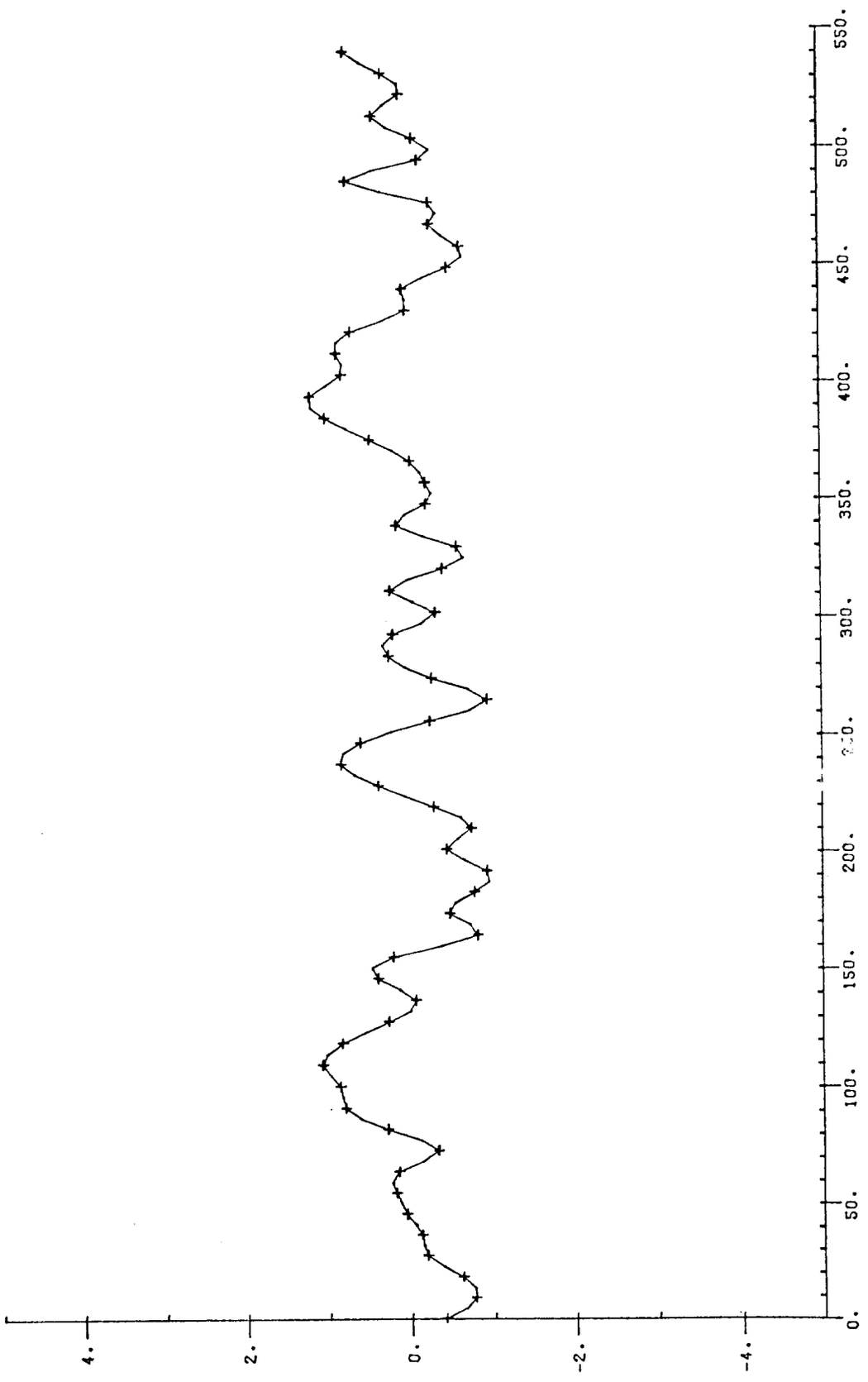


4. Bi-cubic spline interpolation of data (+) along line parallel to y axis (x-grid coordinate 79), for dataset 2

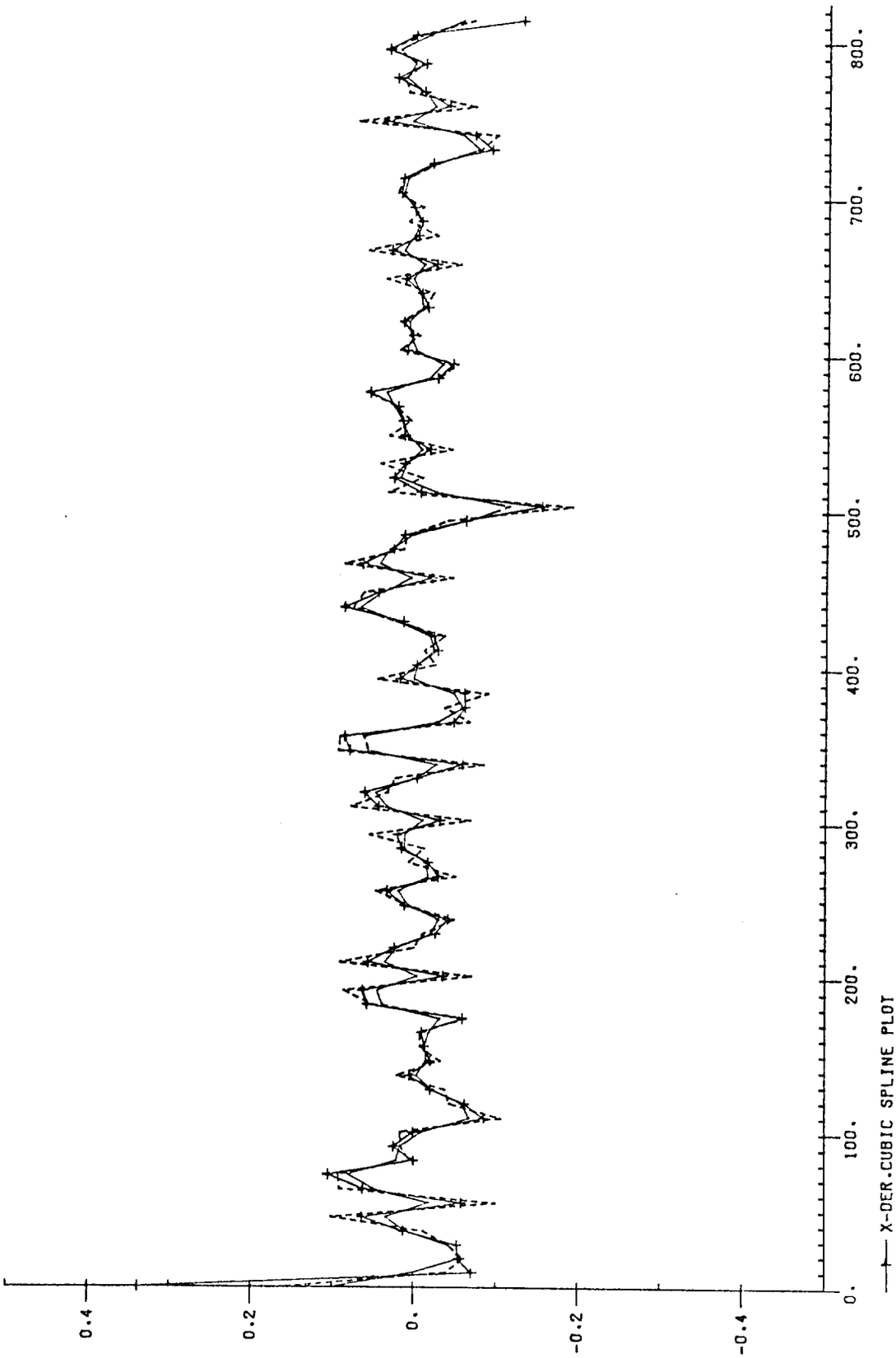


5. x-derivative calculated from data along line shown in figure 3; using linear, Fourier and bi-cubic spline interpolation

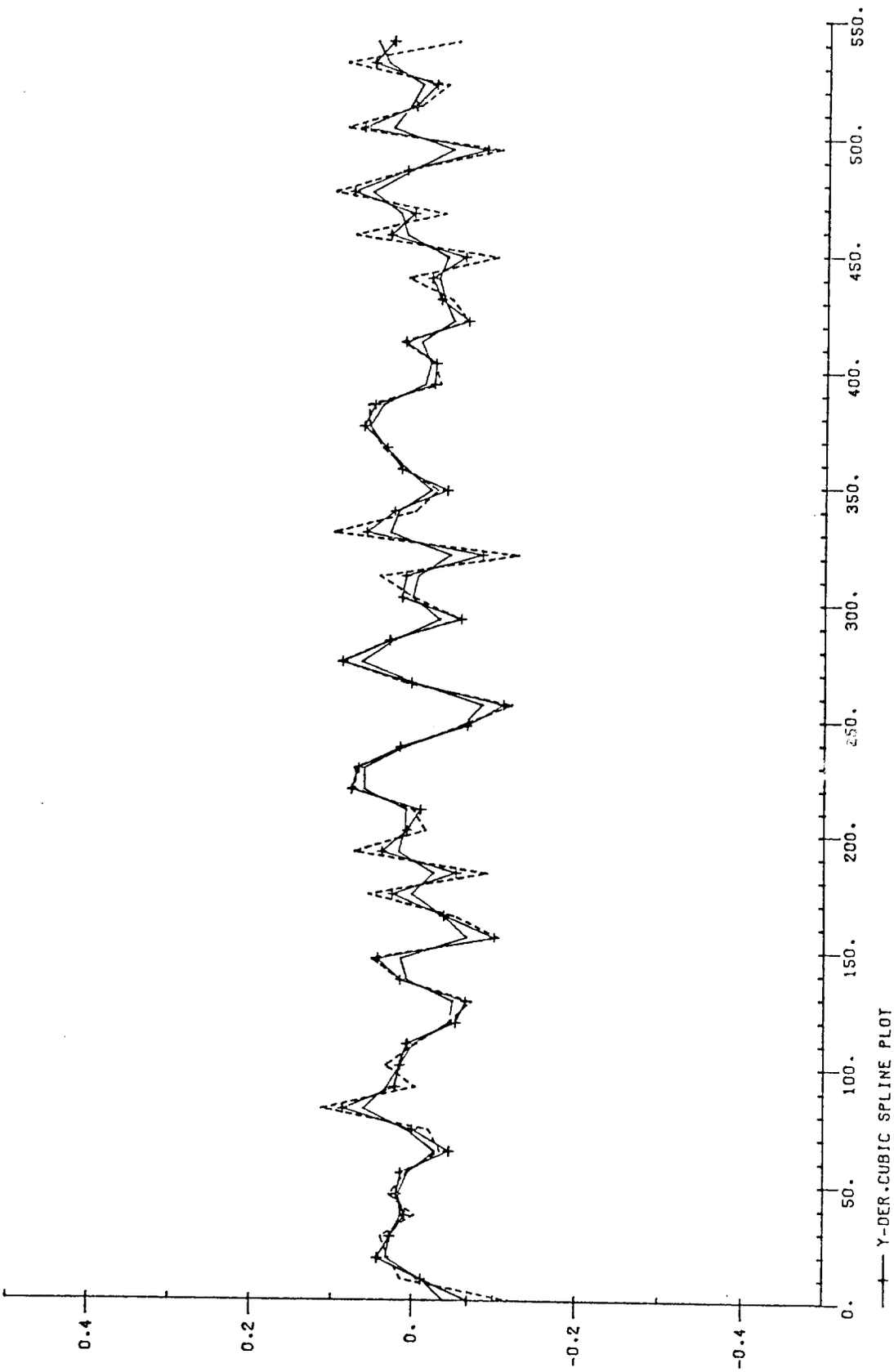


6. y-derivative calculated from data along line shown in figure 4; using linear, Fourier and bi-cubic spline interpolation

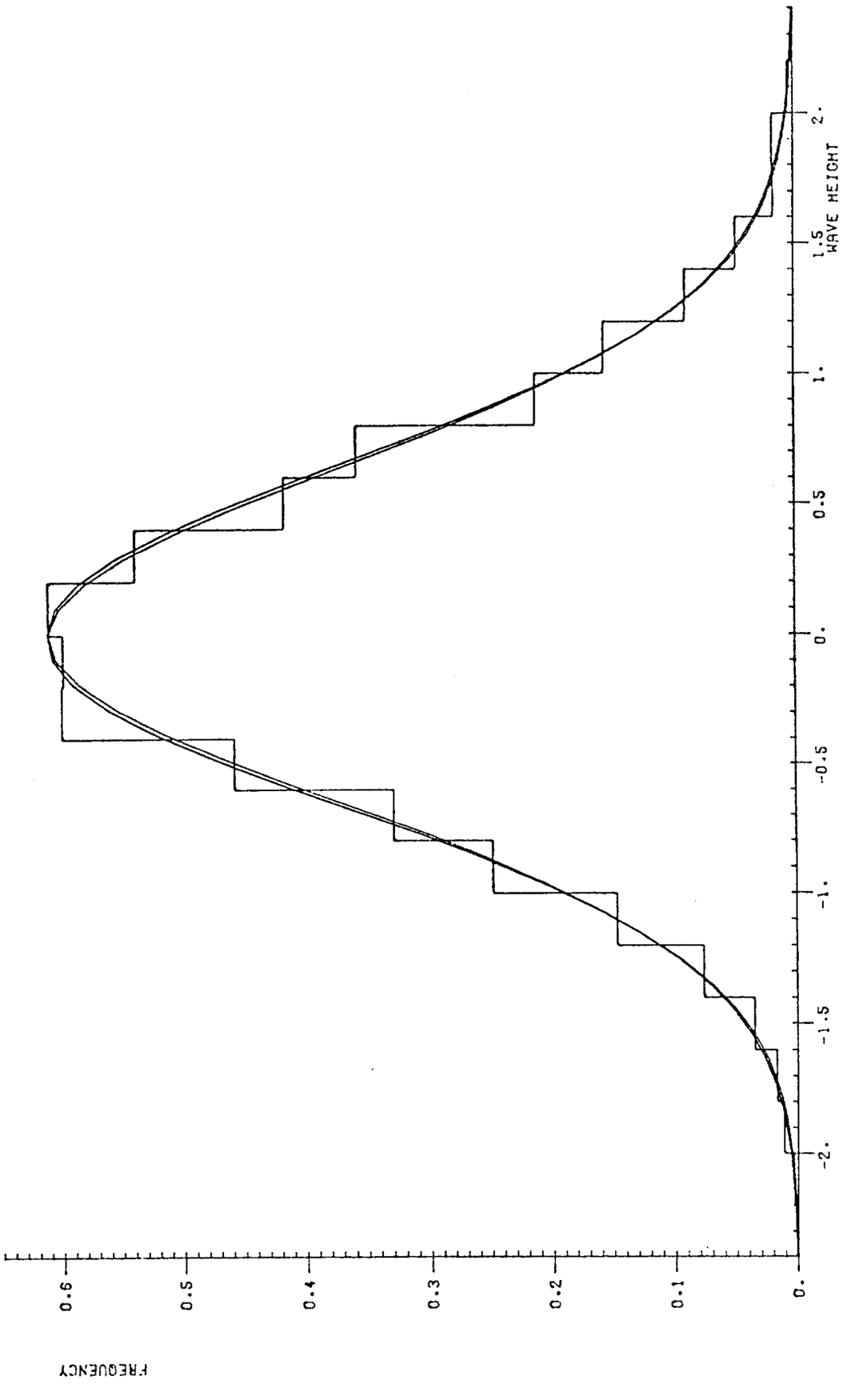


7. Pdf of surface elevation estimated from dataset 2 compared with Gaussian and nonlinear theory

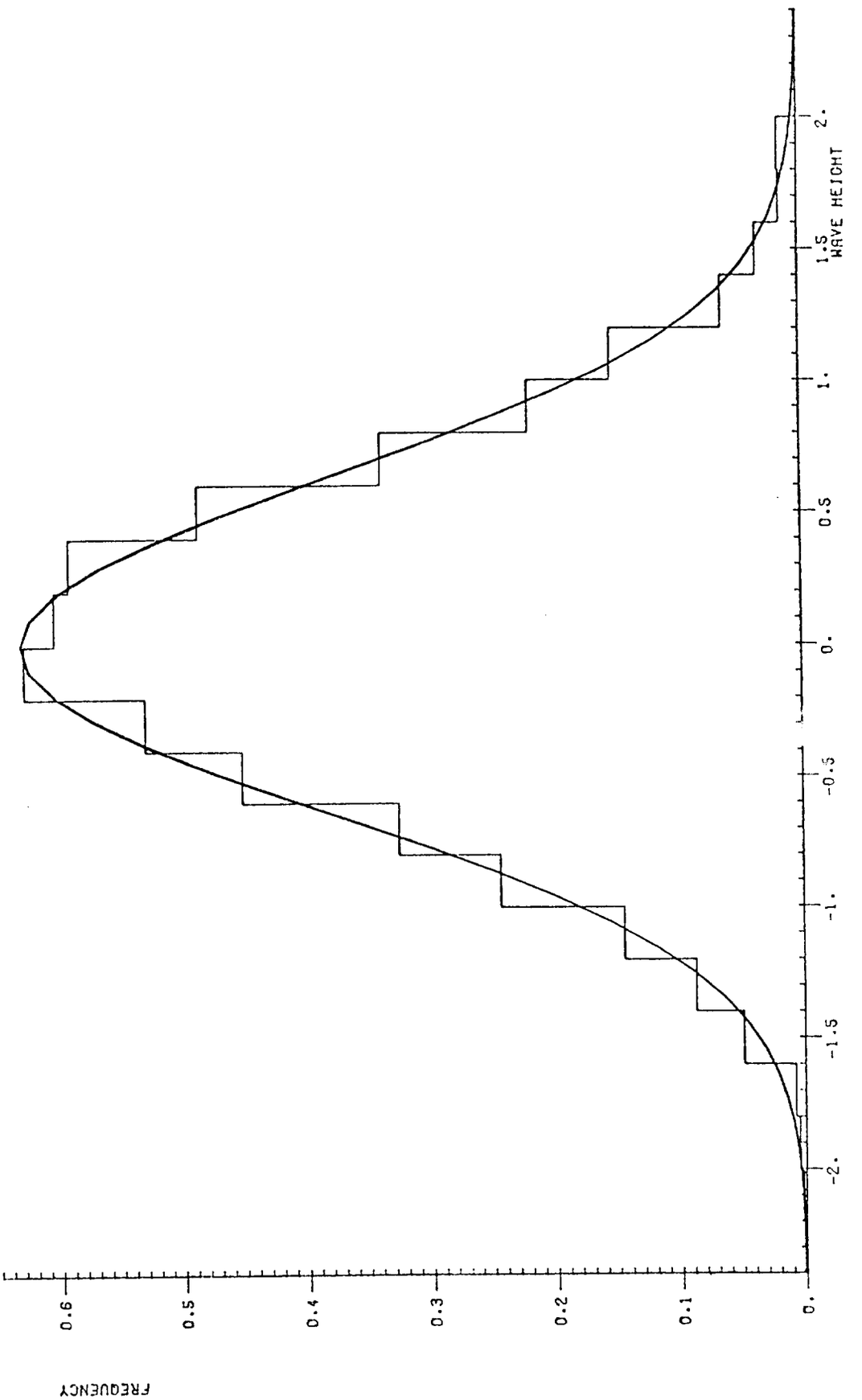


8. Pdf of surface elevation estimated from dataset 3 compared with Gaussian and nonlinear theory

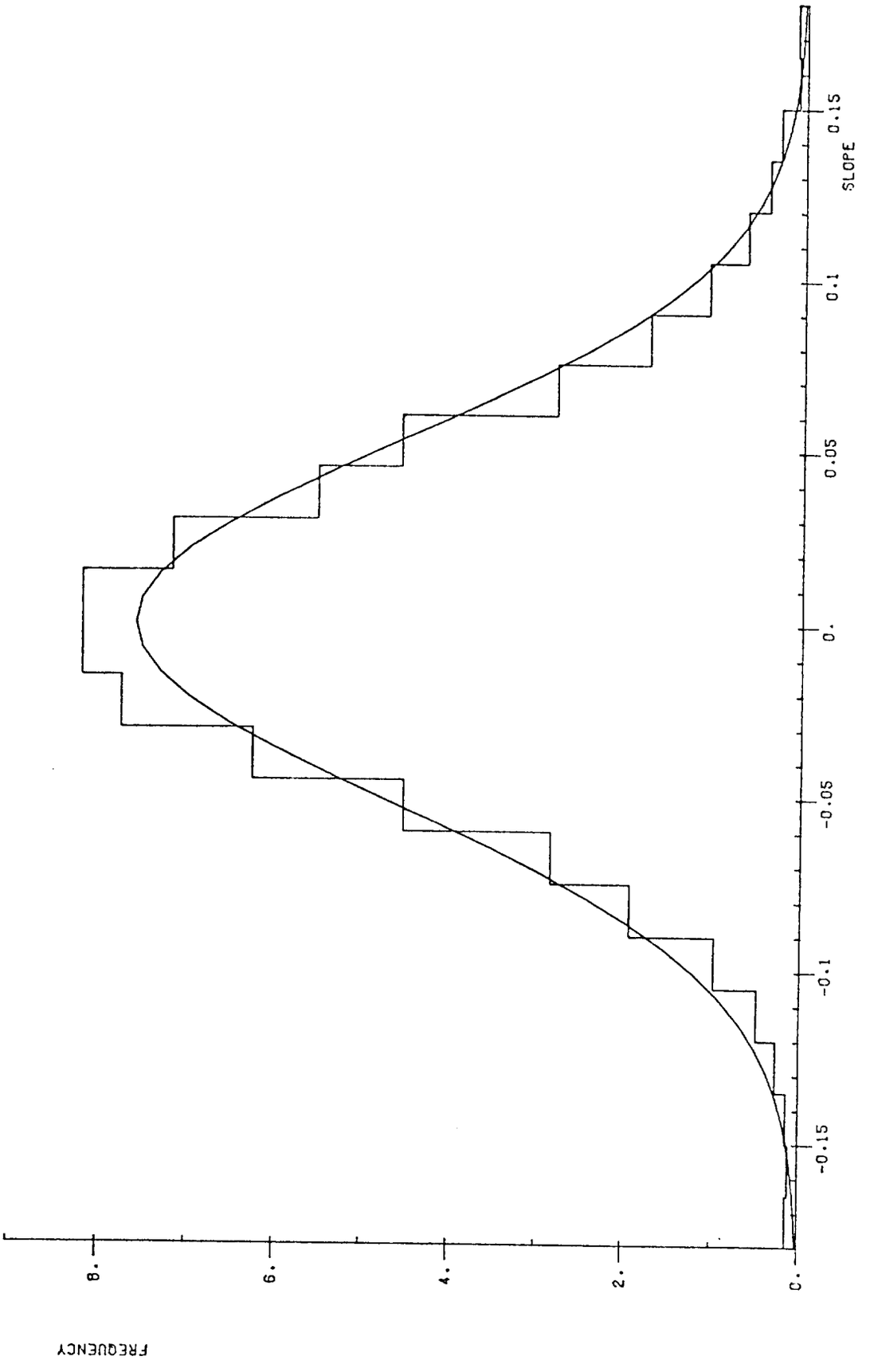


9. Pdf of surface slopes (x derivative) of dataset 2 compared with theoretical curve

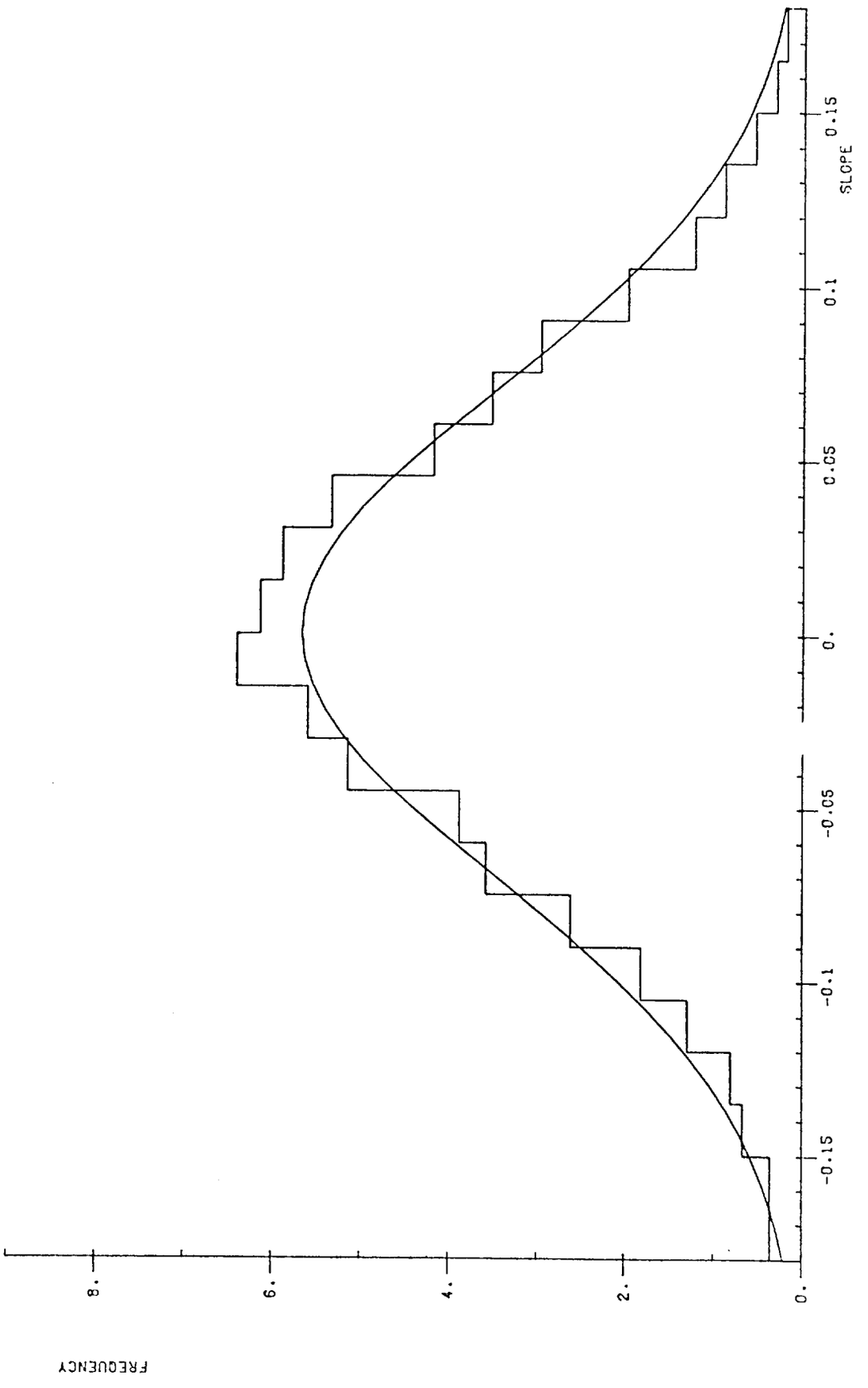


10. Pdf of surface slopes (y derivative) of dataset 2 compared with theoretical curve

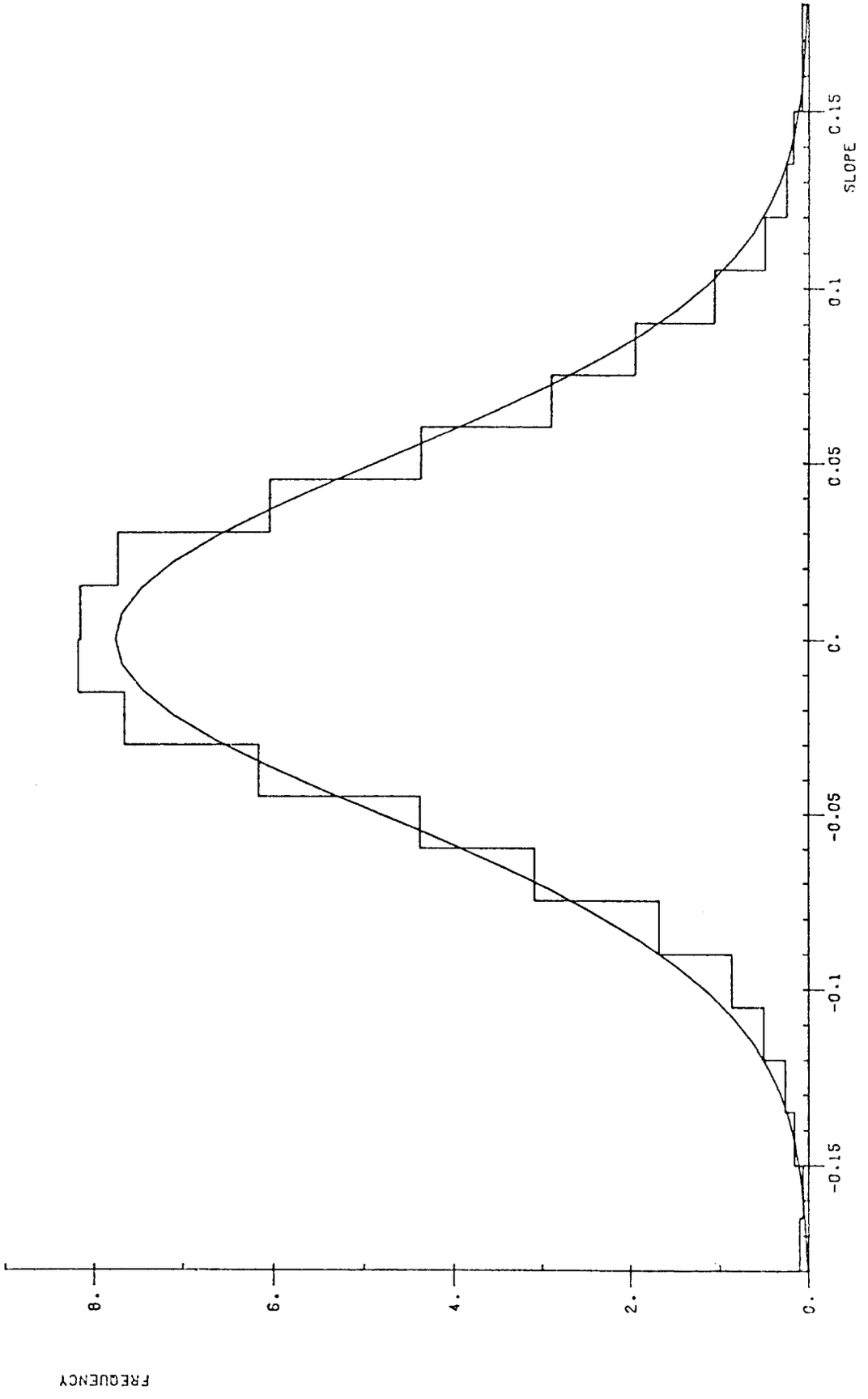


11. Pdf of surface slopes (x derivative) of dataset 3 compared with theoretical curve

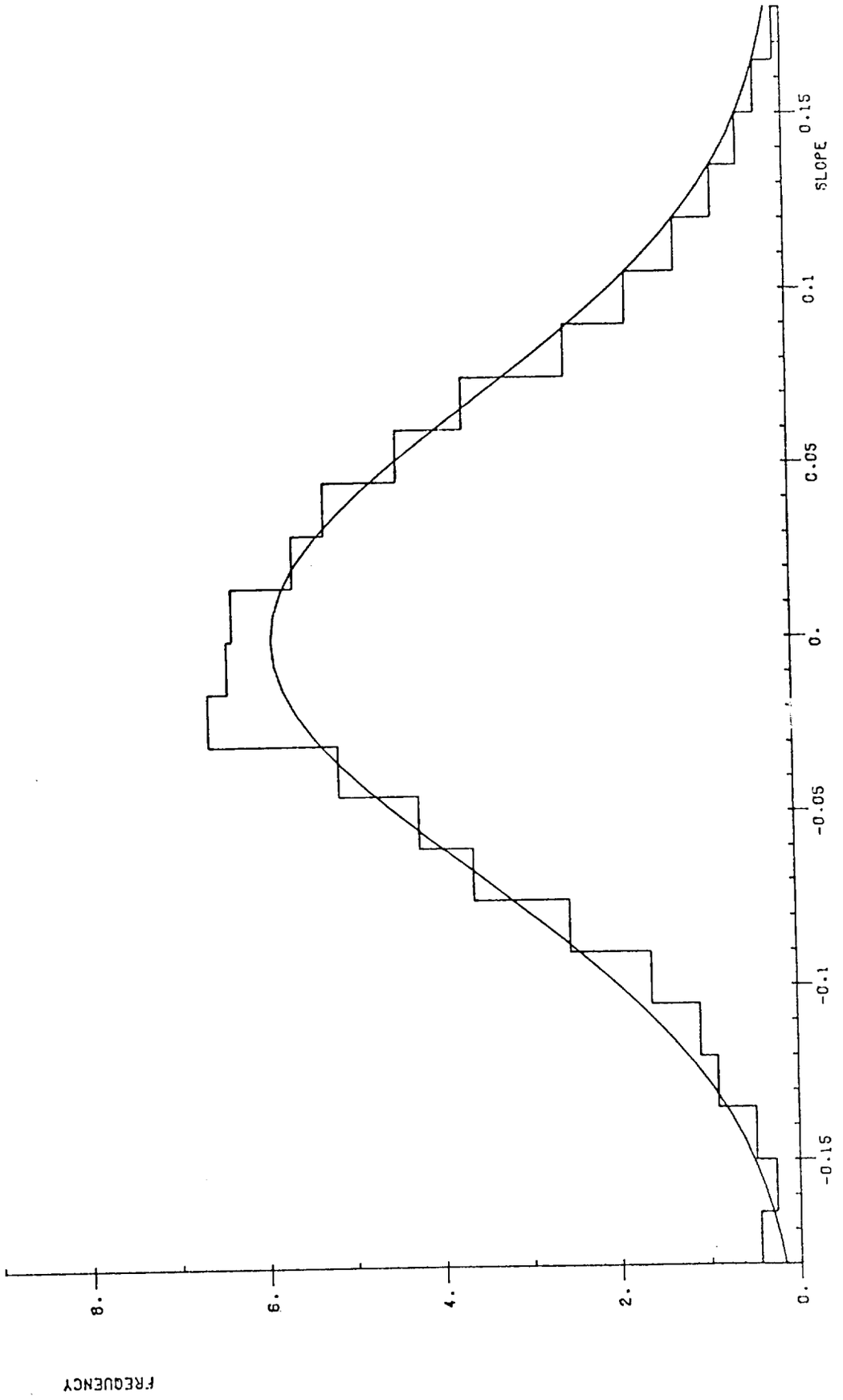


12. Pdf of surface slopes (y derivative) of dataset 3 compared with theoretical curve